Supporting Information

An *Ab Initio* Thermodynamics Study of Cobalt Surface Phases

under Ethanol Steam Reforming Conditions

Wenjia Luo and Aravind Asthagiri

S1. Constructing the general surface phase diagram

To construct the general surface phase diagram for the Co^0/Co^{2+} catalytic system,

we used a method similar to the one applied by Su et al[1].

Consider a CoO_x (x = 0, 1) particle consists of N Co atoms and N*x O atoms, its

stability is determined by both its bulk phase and its surface:

$$\Delta G = N\Delta_f G_{CoO_x} + \Sigma_i \gamma_i A_i \qquad (1)$$

In the above equation, ΔG is the total free energy of the particle; $\Delta_f G_{CoO_x}$ is the Gibbs

formation energy of its bulk phase per CoO_x unit. The subscript i represents each surface

configuration that comprises the surface of the particle; γ_i and A_i represent the surface

free energy and area of that configuration. Both $\Delta_f G_{CoO_x}$ and γ_i dependent on

temperature, p_{H_2O} and p_{H_2}, therefore ΔG also depends on these parameters. The above

relation holds because when we calculate the γ_i for a CoO surface configuration, we used

bulk CoO as an energy reference ($g_{CoO}^{bulk} = \mu_{Co} + \mu_O$), while we used bulk Co as the

energy reference ($g_{Co}^{bulk} = \mu_{Co}$) for Co surface configurations.

In order to compare the stability of two different surface configurations, we

assume that there are two particles which are in the same oxidation states as these two

surface configurations, respectively. We further assume that each particle is fully covered

by one of these two surface configurations. As long as these two particles contain the same number of Co atoms, we can tell which surface configuration is more stable by finding out which particle has lower total free energy. For example, when making a comparison between O-term CoO(111) and OH* adsorbed Co(0001), we can assume that there is a CoO particle covered by the O-term CoO(111) surface (particle 1) and a Co particle covered by the OH* adsorbed Co(0001) surface (particle 2). Both of them contain N Co atoms. Under a particular T, p_{H_2O} and p_{H_2} condition, we can calculate

$\Delta G(1) = N\Delta_f G_{CoO} + \gamma_{O-term\ CoO(111)} A(1)$ and $\Delta G(2) = N\Delta_f G_{Co} + \gamma_{OH*Co(0001)} A(2)$. If $\Delta G(1) < \Delta G(2)$, O-term CoO(111) is more stable under this condition and vice versa.

There are some other assumptions and details that need to be clarified here. Firstly we let $\Delta_f Co = 0$ and expressed $\Delta_f G_{CoO} = \Delta_f G^0_{CoO} - \Delta_f G^0_{H_2O} - RT ln\frac{p_{H_2O}}{p_{H_2}}$ based on the reaction Co + H$_2$O → CoO + H$_2$. $\Delta_f G^0_{CoO}$ and $\Delta_f G^0_{H_2O}$ were obtained from thermodynamics tables[2]. Secondly, we assumed that the particles are spherical. Densities of Co and CoO are 0.0908 and 0.0517 Co atoms/Å^3, respectively. Therefore their surface areas can be calculated when the number of Co atoms is given. Thirdly, from experimental results we found that the sizes of Co/CoO particles under ESR conditions are usually in the order of 10^2 Å$^{3-5}$. Thus we estimated the number N of Co atoms in each particle to be approximately 5×10^4, and the surface areas of Co and CoO particles to be 3.25×10^4 and 4.73×10^4 Å^2, respectively. Therefore all parameters in eqn. (1) are given and the stability of surface configurations can be compared by their ΔG values calculated from eqn. (1).

S2. The surface phase diagrams at different temperatures

In this study, since we considered the vibrational and entropic contributions from surface adsorbates, free energies of surface slabs depend on temperature as well as gas phase H_2O and H_2 molecules. In addition to the typical ESR temperature of 723 K discussed in the paper, we also plotted the surface phase diagrams at 523 and 923 K, as shown in the following two figures, to see how the surface structures change if the ESR reactions are operated at a lower or higher temperature.

From the general surface phase diagram, several observations can be drawn.
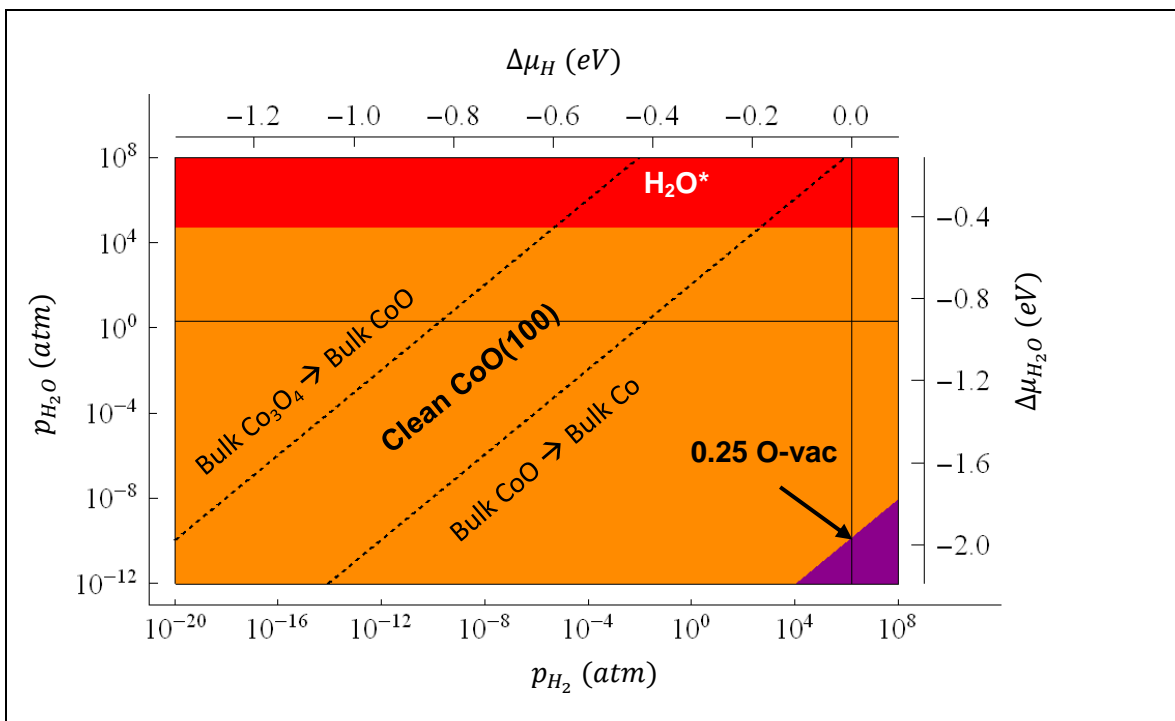
The temperature has a weak influence on the transition from CoO surfaces to metallic Co surfaces. This observation can be explained by the fact that as the temperature raises from 523 to 723 and 923 K, $\Delta_r G^0$ for Co + H_2O → CoO + H_2 only slightly increases from 0.217 to 0.259 and 0.292 eV. As a result, both the transition from CoO(100) to Co(0001) and the transition from 1.0 OH* CoO(111) to OH* Co(0001) approximately occur when $\frac{p_{H_2O}}{p_{H_2}} = 10^2$ at all temperatures. On the other hand, the equilibrium between CoO and Co_3O_4 depends more strongly on the temperature, since $\Delta_r G^0$ for 3CoO + H_2O → Co_3O_4 + H_2 increases from 1.045 to 1.290 and 1.533 eV as the temperature changes from 523 to 723 and 923 K. However since chemical potentials of H_2O and H also depend on the temperature, and the condition under which CoO is more stable than Co_3O_4 can be expressed as $\frac{p_{H_2O}}{p_{H_2}} < exp(\frac{\Delta_r G^0}{RT})$, the $\frac{p_{H_2O}}{p_{H_2}}$ ratio at which CoO and Co_3O_4 are at equilibrium in the bulk phase actually decreases from 1.17×10^{10} to 9.75×10^8 and 2.33×10^8 atm as the temperature goes up from 523 to 723 and 923 K.

Therefore at a given p_{H_2O} and p_{H_2}, a lower temperature actually favors the stabilization of CoO against oxidation into Co_3O_4.
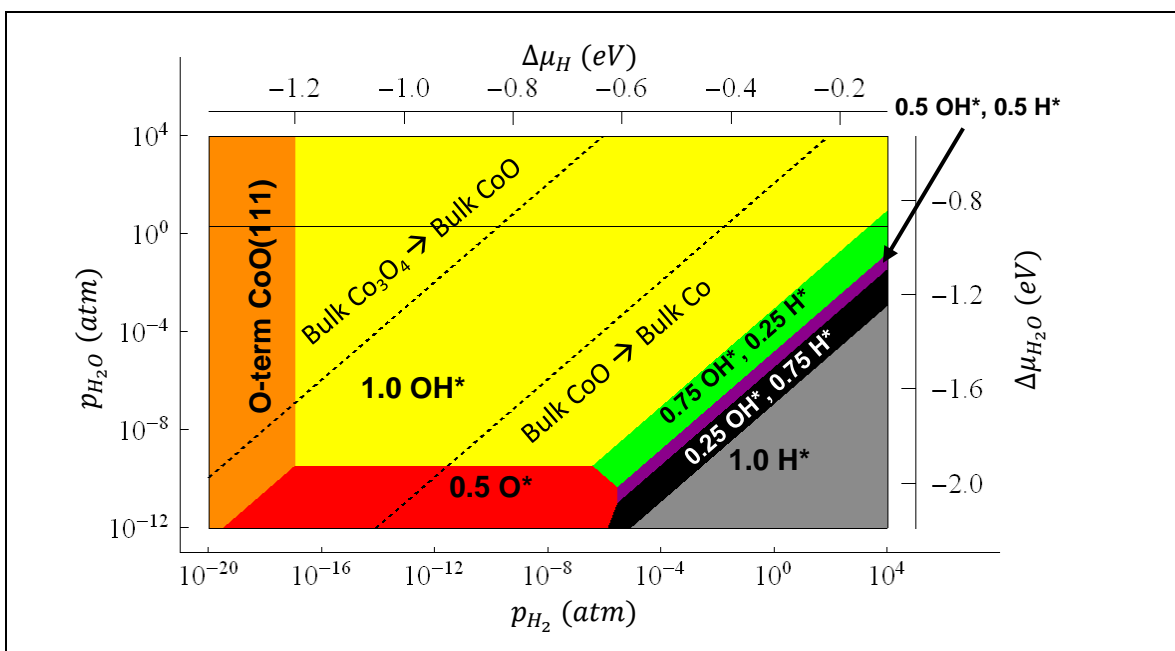
For the CoO(100) facet, lower temperature facilitate the molecular adsorption of H_2O, but it also disfavors the formation of oxygen vacancies or H_2O dissociation into OH* and H*. However under ESR reaction conditions the most stable configure is still the clean CoO(100) surface.

For the CoO(111) facet, lower temperature favors the OH* adsorption or OH*, H* mixed adsorption on the surface. As temperature rises, O-term CoO(111) with or without oxygen vacancies become the stable configurations when p_{H_2O} and p_{H_2} are low.
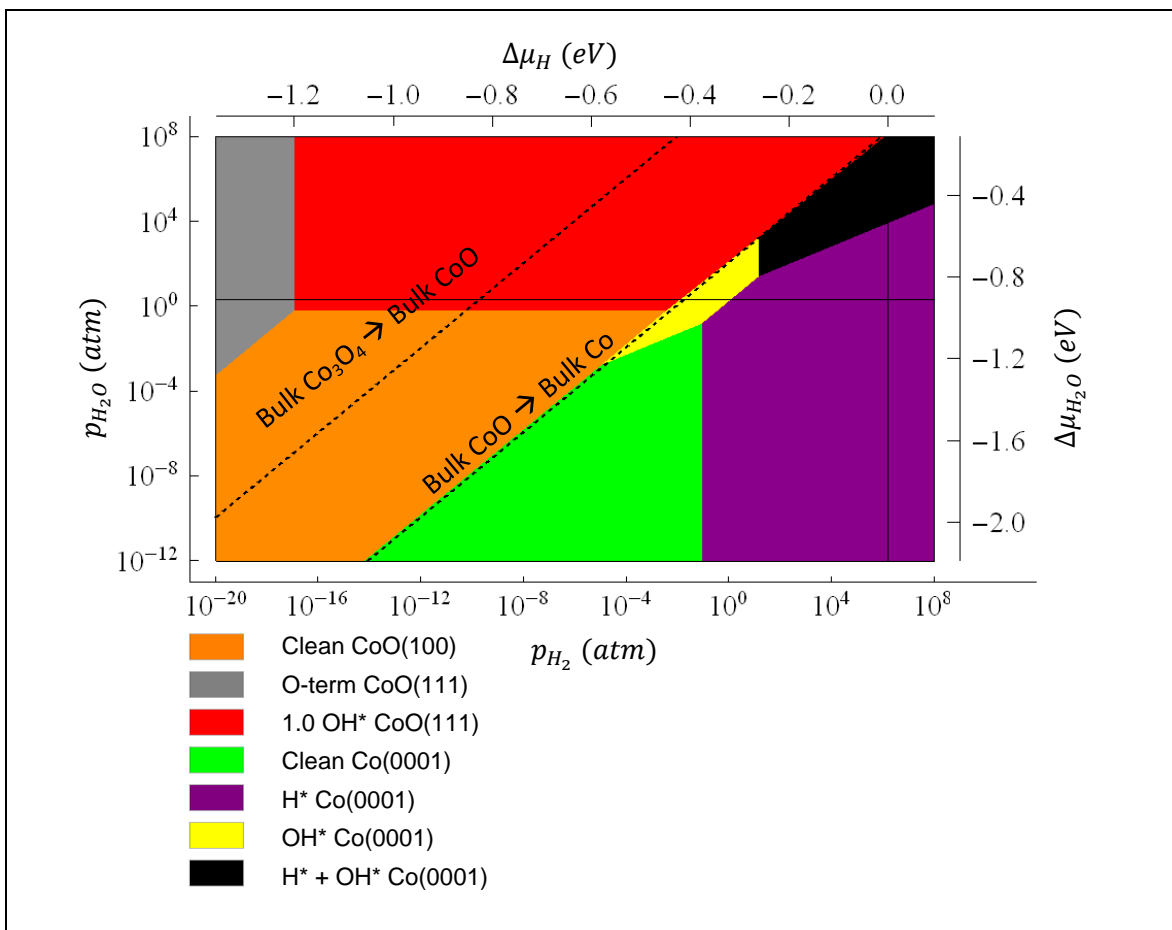
In summary, temperature has a relatively weak influence on the surface phase diagrams of Co^0/Co^{2+} catalysts. Conclusions drawn in this paper may also apply to situations where the temperature is slightly higher or lower (± 200 K) than 723 K.

(a)

(b)

Legend:
- Clean CoO(100) (orange)
- O-term CoO(111) (gray)
- 1.0 OH* CoO(111) (red)
- Clean Co(0001) (green)
- H* Co(0001) (purple)
- OH* Co(0001) (yellow)
- H* + OH* Co(0001) (black)

Axis labels: $\Delta\mu_H$ (eV), p_{H_2O} (atm), $\Delta\mu_{H_2O}$ (eV), p_{H_2} (atm)

In-figure labels: Bulk Co$_3$O$_4$ → Bulk CoO, Bulk CoO → Bulk Co
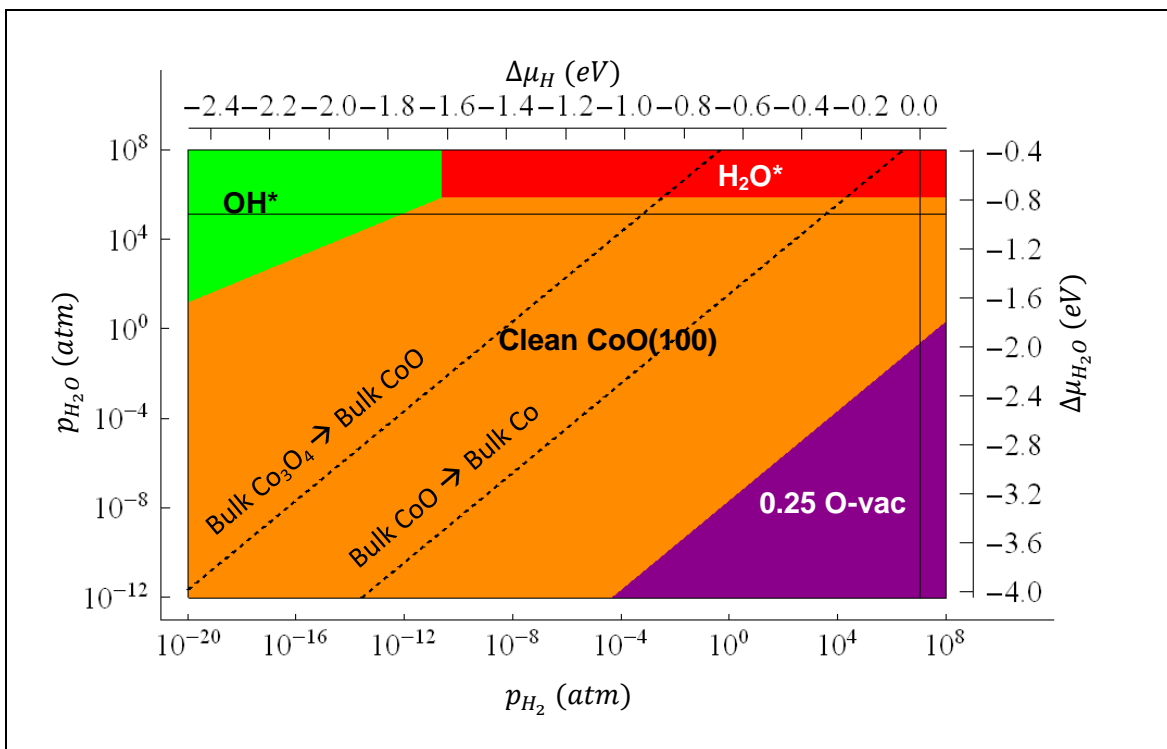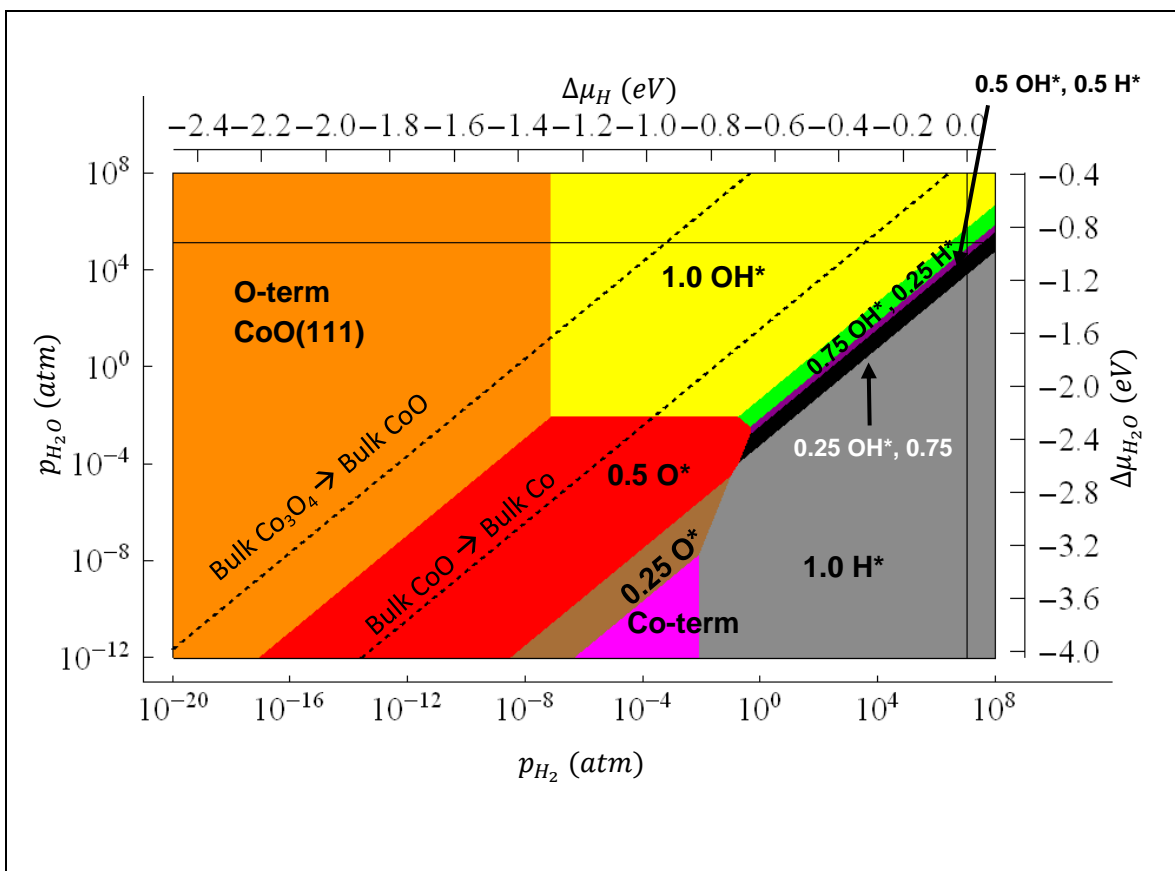
(c)

Fig. S1. Surface phases diagrams at 523 K for (a) CoO(100), (b) CoO(111), and (c) general Co^0/Co^{2+} catalyst. The black solid and dashed lines in this figure have the same meaning as those presented in Fig. 3 in the paper.
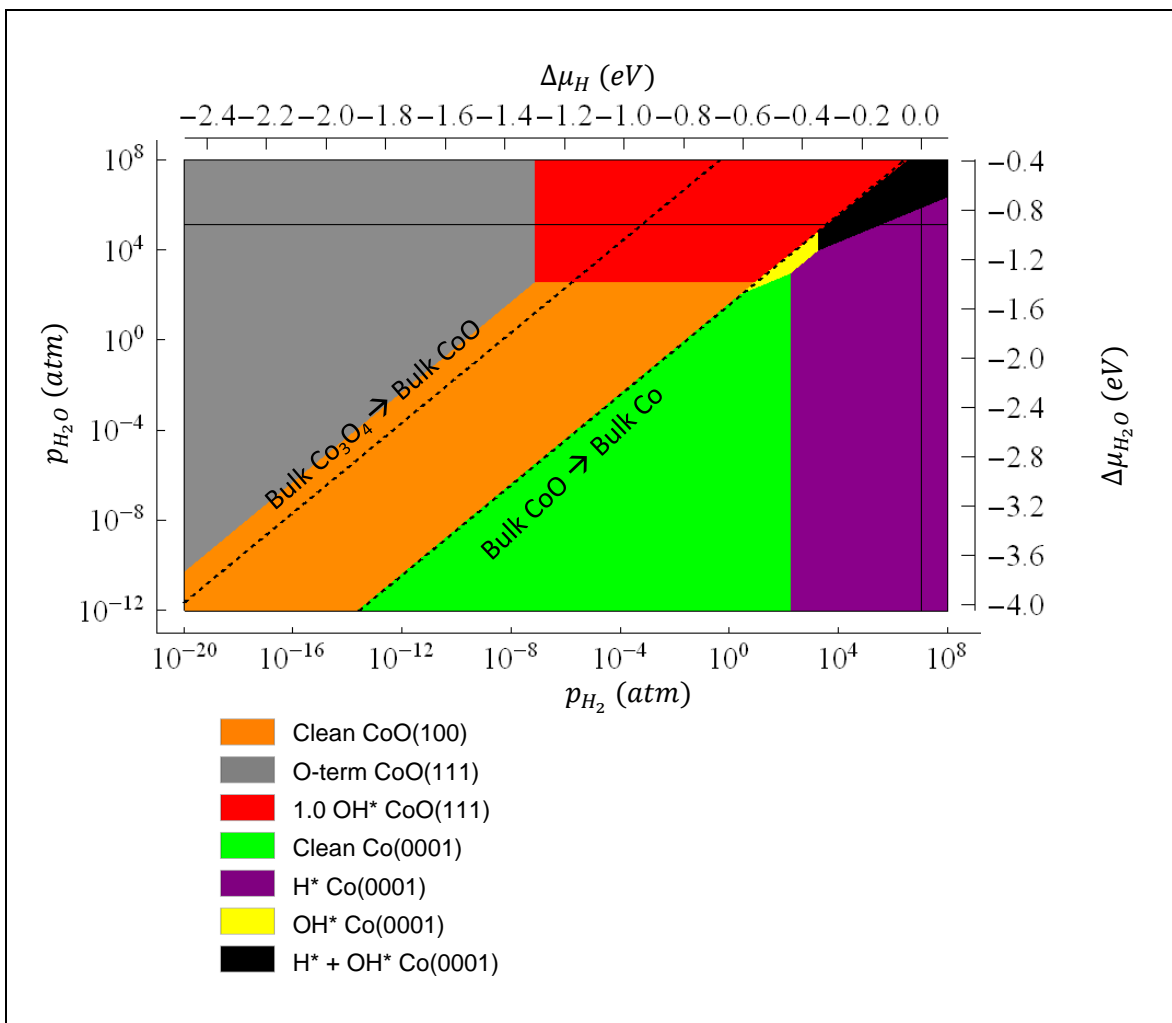
(a)

(b)

(c)

Fig. S2. Surface phases diagrams at 923 K for (a) CoO(100), (b) CoO(111), and (c) general Co^0/Co^{2+} catalyst. The black solid and dashed lines in this figure have the same meaning as those presented in Fig. 3 in the paper.

S3. Influence of magnetic moments configuration

The results presented in the paper were based on the antiferromagnetic ground state of CoO. However as mentioned in the Method section, under ESR reaction conditions the CoO material should be paramagnetic. Without the antiferromagnetic ordering of magnetic moments in the CoO structure, our results could lead to large errors.

To address this issue, we re-did some of the calculations by breaking the antiferromagnetism of CoO. Specifically, we tested several typical surface configurations for both the (100) and (111) facets of CoO. Reaction energies that are needed to convert one configuration to another one were calculated based on various magnetic moments configurations that are non-antiferromagnetic. Results of these calculations are given in Table S1. In antiferromagnetic configuration (AFM), within each unit cell there are 2 up-spin and 2 down-spin Co atoms on each layer; In "Para 1" configuration listed in Table 4, there are 3 up-spin and 1 down-spin Co atoms on the 1st layer; in "Para 2", 1 up and 3 down on the 1st layer; in "Para 3", 4 up and 0 down on the 1st layer; in "Para 4", 3 up and 1 down on the 2nd layer. Other Co atoms not specified here are with the same magnetic configuration as AFM. Reaction energies of these reactions for AFM CoO were previously given in Table 1 and 2 but are also listed here for ease of comparison.
As is evident from Table S1, relative stability between different surface configurations usually varied within 0.1 eV compared with the AFM configuration, which is equivalent to an variation of 2-4 meV/Å and is considered to be small in this study. Thus we conclude that although the absolute values of surface free energies will increase due to a paramagnetic configuration (since AFM is the most stable magnetic configuration),

relative stability of different surface configurations, as well as the conclusions drawn in

this paper, are not likely to be changed.

Table S1. Reaction energies (eV) on CoO(100) and CoO(111) with various magnetic moments configurations.

Facet	Reaction	AFM	Para 1	Para 2	Para 3	Para 4
(100)	Clean + H$_2$ → 0.25 O-vac + H$_2$O	1.79	1.76	1.75	1.71	1.80
	Clean + H$_2$O → H$_2$O*	-0.39	-0.45	-0.48	-0.40	-0.46
	H$_2$O* → OH* + H*	2.75	2.86	2.87	2.78	2.74
(111)	1.0 OH* + H$_2$ → 0.75 OH*, 0.25 H* + H$_2$O	0.39	0.40	0.37	0.51	0.40
	0.75 OH*, 0.25 H* + H$_2$ → 0.5 OH*, 0.5 H* + H$_2$O	0.62	0.64	0.71	0.59	0.70
	0.25 OH*, 0.75 H* + H$_2$ → 1.0 H* + H$_2$O	0.88	0.92	0.81	1.00	0.86

S4. Ethanol dehydrogenation on CoO

Although we did not explore the ESR reaction pathways on CoO surfaces in this paper, we examined the first step of ESR, i. e. ethanol dehydrogenation, on the most stable surface configurations of CoO(100) and CoO(111). Table S2 shows the reaction energies of ethanol dehydrogenation on clean CoO(100), 1.0 OH* CoO(111), and 1.0 OH*, 0.25 H* CoO(111). Fig. S3 shows the corresponding structures of EtO* adsorbed on CoO surfaces.

Table S2. Ethanol dehydrogenation reaction energies (eV) on CoO(100) and CoO(111) with various surface configurations. The geometry of these products are shown in Fig. S3.

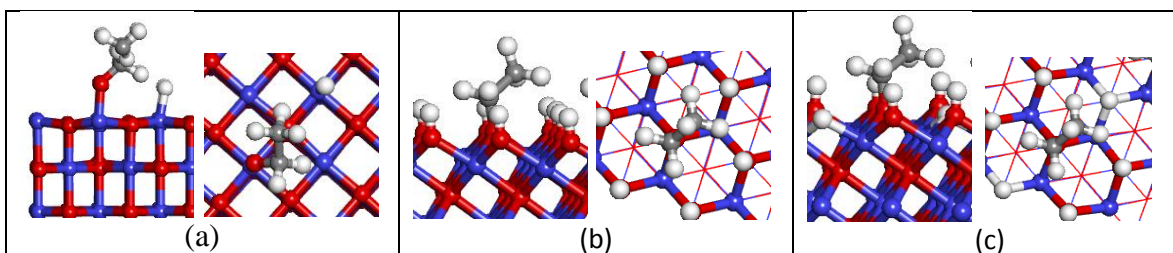| Facet	Reaction	ΔE (eV)
(100)	Clean + EtOH → EtO* + H*	2.64
(111)	1.0 OH* + EtOH → 0.25 EtO* 0.75 OH* + H_2O	0.17
	0.75 OH*, 0.25 H* + EtOH → 0.25 EtO* 0.25 H* 0.5 OH*+ H_2O	0.10

Fig. S3. Geometry of ethanol dehydrogenation products on various CoO surfaces. (a) EtO* and H* on clean CoO(100). (b) 0.25 EtO*, 0.75 OH* CoO(111). (c) 0.25 EtO*, 0.25 H*, 0.5 OH* CoO(111)

Ethanol dehydrogenation, similar to H_2O dissociation, is very endothermic on CoO(100), but almost thermoneutral on 1.0 OH* CoO(111) or 0.75 OH*, 0.25 H* CoO(111). At the first inspection of Fig. S3(b), one may think that other OH* groups presented on the surface (especially the one close to the CH_3 group on EtO) can pose

steric hindrance to the EtO group, thus making this structure unstable. In Fig. S3(c), the OH* group most close to the CH_3 group is replaced by a much smaller H* atom. As a result, the EtOH dehydrogenation becomes more favored by 0.07 eV. However the decrease in reaction energy due to replacement from OH* to H* is quite small, suggesting that the steric hindrance posed by the OH* groups on EtO*, if present, is not significant.

However the above discussion is only based on thermodynamics. Kinetically, surface adsorbed OH* groups may influence the dehydrogenation of ethanol. On one hand, OH* groups can lower the O-H bond breaking barriers by stabilizing the transition states through hydrogen bonds[6, 7], thus making the dehydrogenation of ethanol more favored. On the other hand, if the CoO(111) surface is fully covered by OH* groups, they can block the CoO surface and prevent ethanol having contact with the surface. To quantitatively predict the overall effect, a competitive adsorption model can be built to estimate the surface coverages of OH* and EtO* under ESR reaction conditions[8]. However since we showed that substituting an OH* with an EtO* is almost thermoneutral and OH* groups do not pose much steric hindrance, it is unlikely that OH* can prevent the surface from reacting with ethanol. Therefore we would predict that ethanol dehydrogenation is more favored on CoO(111) than on CoO(100).

References

1   H.-Y. Su, Y. Gorlin, I. C. Man, F. Calle-Vallejo, J. K. Norskov, T. F. Jaramillo and J. Rossmeisl, *Phys. Chem. Chem. Phys.*, 2012, **14**, 14010-14022.
2   M. W. Chase, *NIST-JANAF thermochemical tables*, 4 edn., American Institute of Physics, 1998.
3   H. Song and U. S. Ozkan, *J. Catal.*, 2009, **261**, 66-74.
4   H. Song, B. Tan and U. S. Ozkan, *Catal. Lett.*, 2009, **132**, 422-429.
5   J. Llorca, P. R. de la Piscina, J.-A. Dalmon, J. Sales and N. Homs, *Appl. Catal., B*, 2003, **43**, 355-369.
6   C. Michel, F. Auneau, F. Delbecq and P. Sautet, *ACS Catal.*, 2011, **1**, 1430-1440.
7   S. Lin, R. S. Johnson, G. K. Smith, D. Xie and H. Guo, *Phys. Chem. Chem. Phys.*, 2011, **13**, 9622-9631.
8   A. A. Phatak, W. N. Delgass, F. H. Ribeiro and W. F. Schneider, *J. Phys. Chem. C*, 2009, **113**, 7269-7276.